HEAVY MINERAL DIAGNOSIS OF RAS BAGHDADY BLACK BEACH SAND: ACCUMULATIONS AND SIGNIFICANCE

SAKR S.[1], EL-AFANDY A. H.[2], ABU HALAWA A. F.[2], AWAD M. E.[1]

1-Al-Azhar Univ., Sci. Fac., Geology Dept., 2- Egyptian Nuclear materials authority

Abstract

A total of 30 samples each weighs 5 kg were collected from digging boreholes at 2 m depth at constant intervals across three profiles from Ras Baghdady beach sands, Red Sea coast, Egypt. Sieving, heavy mineral separation using Wilfy Shaked table and heavy liquid, magnetic separation using Lift type separator, mineral picking, mineral identifications, XRD, EDX and BSE have been performed to reveal the different mineral groups and the economic potentials. The separated grain size sub-samples arranged in their p order of abundance are 0.25-0.125 mm (10-60%), 0.5-0.25 mm (<10 to 20%), and 0.125-0.063 mm (<5 to 10%). Moreover, less than 1% to 10% are randomly distributed between grain size fractions < 0.063 and 1-0.5 mm. The most promising fraction based on the microscopic investigations containing mineral varieties and groups is very fine sand size. 60 gm of pure heavy minerals produced from 600 gm very fine sand size (0.125-0.063 mm). The light minerals are mainly detrital quartz grains and feldspars with mica flakes while the heavy minerals submitted to magnetic separation. Four separated magnetic sub-fractions (magnetite, ilmenite I, ilmenite II and ilmenite III) and one non-magnetic sub-fraction are obtained. The separated heavy minerals from Ras Baghdady very fine sand size (0.125-0.063 mm) contain 90 % of green silicates and 10 % of other heavy minerals in which ilmenite reaches 52 %, magnetite up to 15 %, garnet up to 11 %, goethite up to 11 %, zircon up to 5 %, rutile up to 3 %, sphene up to 3 % and other recorded traces of combined minerals up to 2 %. Based on the stereoscopic vision, XRD, BSE and SEM investigations, most of the studied heavy mineral grains are angular to sub-angular and homogenous in composition with a few variations to reflect short distance transportation and low energy deposition as depicted from the magnetically separated ilmenite grade III. The relative abundance and lateral distribution of the economic heavy mineral assemblages in the studied area are mainly controlled by hydraulic effects and beach topography. The estimated reserve of the economic heavy minerals within Ras Baghdady beach very fine sand can be summed up as follows; ilmenite 23490 tons, magnetite 6710 tons, garnet 5070 tons, goethite 5140 tons, zircon 2170 tons, rutile 1220 tons, sphene 1490 tons and leucoxene 10 tons. In addition to first record of ruby and sapphire, rare metal and radioactive bearing minerals such as monazite in which rare earth elements range is 61.2%, ~ 6.70 % Th, and ~ 5.4 % U as well as high content of Nd (17. 3%) and Sm (4.37%) are also recorded. Furthermore, the semi-quantitative EDX analyses of the picked uranothorite grains show high content of Th (40.12 %), U (11.77 %), and Y (11.9 %) while xenotime contains high content of Y2O3 (25.53 %), Yb2O3 (4.97 %), Nd2O3 (4.19 %) and Ce2O3 (3.46 %) as well.

Introduction

The present article is established to shed light on the heavy mineral assemblages and their economic potential recorded in the black beach sands accumulated at Ras Baghdady area. Ras Baghdady is located on the Red Sea coastal plain, 50 kms south of Mersa Alam, between longitude 35˚ 05´ 24˝ & 35˚ 05´ 54˝ E. and latitude 24˚ 38´ 34˝ & 24˚ 40´ 18˝ N. Ras Baghdady covers nearly 5.5 km^2 and ends downstream of Wadi El-Gemal in inverted deltoid shape to the beach (Fig. 1).

Wadi (W.) El Gemal, the upper reaches of the studied area is covered with high to moderate relief, rugged topographic mountainous terrains that characterize the basement complex of the Nubian Shield outcropping in Eastern Desert of Egypt.
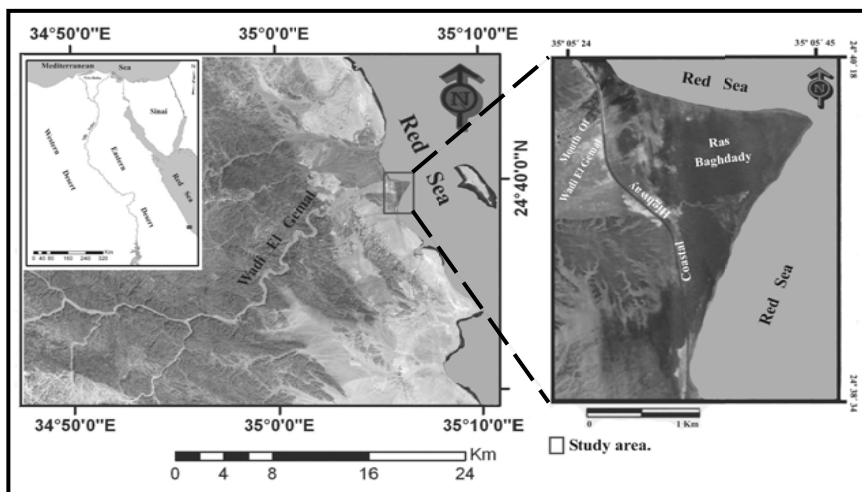
Fig. (1): Location map of the study area.

Meanwhile, Wadi El Gemal drainage patterns as one of the predominant old river systems in the southern part of Egyptian Eastern Desert drained through the basement rocks toward the Red Sea with chief tributaries W. Nugrus, W. Hangaliya, W. Sakait and W. Abu Rusheid (Fig. 2). Moreover, Wadi El Gemal floor is covered with reworked Quaternary sediments derived from igneous and metamorphic rocks hosting deposits chiefly sulphides and oxides. These rocks are exposed as conspicuous outcrops on both sides of these drainage patterns. These rock units are studied and classified by many authors (El Shazly and Hassan,1972, Saleh,1997, Assaf et al., 2000, Khalid, 2005 and Hassaan, 2011). Accordingly, these rock units arranged from the oldest to the youngest are psammitic gneiss, hornblend gneiss, schist, mafic and ultra-mafic dismembered ophiolitic rocks, basic to intermediate metavolcanics, granodiorites, biotite granite, muscovite-plagioclase granite, post granitic dykes, pegmatites, aplite and quartz veins. These basement rocks are unconformably covered with Miocene, Pliocene and pleistocene sediments in the east ward direction toward the Red Sea (Fig. 3).

In this province, arid climatic conditions prevail where, the annual ranges of temperatures are 36º - 18º and 60º - 40º respectively. The day-night temperature drops from 45 to 10 °C, and low sediments reworking is manifested due to the lack of rain fall precipitation. The effective wind directions on Red Sea coast are NW, N and NE. Meanwhile, the southern winds are seasonal and have no effect. However, sustainably heavy rains occasionally occur transferring a huge amount of weathering products to the Red Sea coast. These transportation processes are off course controlled by the gradients, whereas the increasing in slope permits a huge quantity of loose sediments to transfer toward the Red Sea coast and even to the continental shelf forming accumulated clastic sediments. Subsequently, these sediments are washed and concentrated by the action of Sea waves, turbidity currents and tidal currents. In this respect, the fine grains are transported for long distances by natural processes than the coarse grains. In contrast, large mineral grains are not transported far before coming

to precipitated in a depositional basin and those are not as diagnostic as smaller grains. Therefore, small particles of heavy minerals are good clues to sediment provenance, transportion, and distribution.
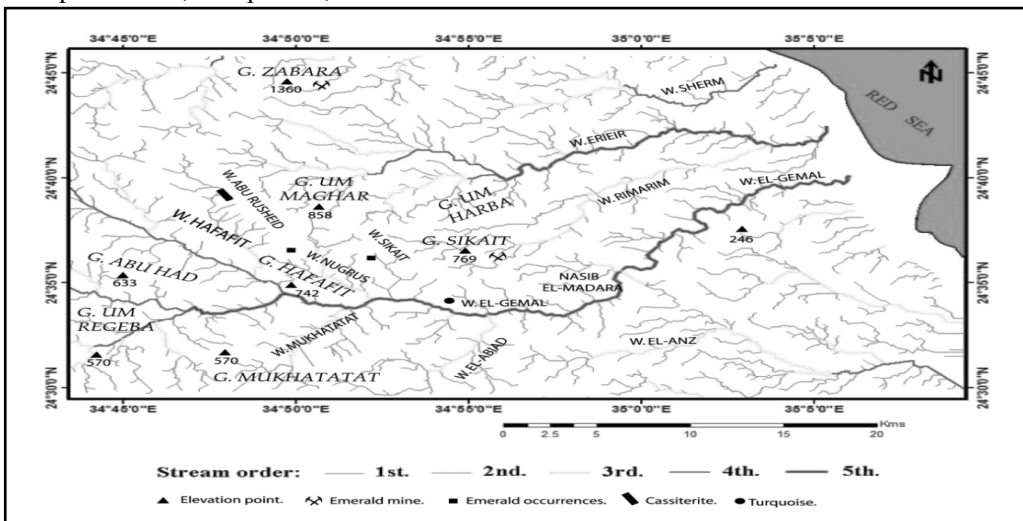

Fig. (2): Drainage pattern map of Wadi El Gemal basin.

These transported loose sediments consist chiefly of light constituents with presence of heavy mineral constituents. The light mineral constituents are quartz, feldspars, and lithic fragments, while the heavy minerals contain several mineral groups with densities greater than 2.85 g/cm^3. The heavy mineral groups include several varities such as ilmenite and leucoxene, rutile, zircon, monazite and xenotime, kyanite, sillimanite and andalusite, staurolite, garnet, chromite, magnetite, cassiterite, columbite-tantalite, wolframite, scheelite, as well as precious metals and gem stones (See Kitaisky, 1963, Dill, 1998 and Wong, 2001). Furthermore, the heavy minerals reflect the nature of source rock area because different rock types contain different heavy mineral associations.
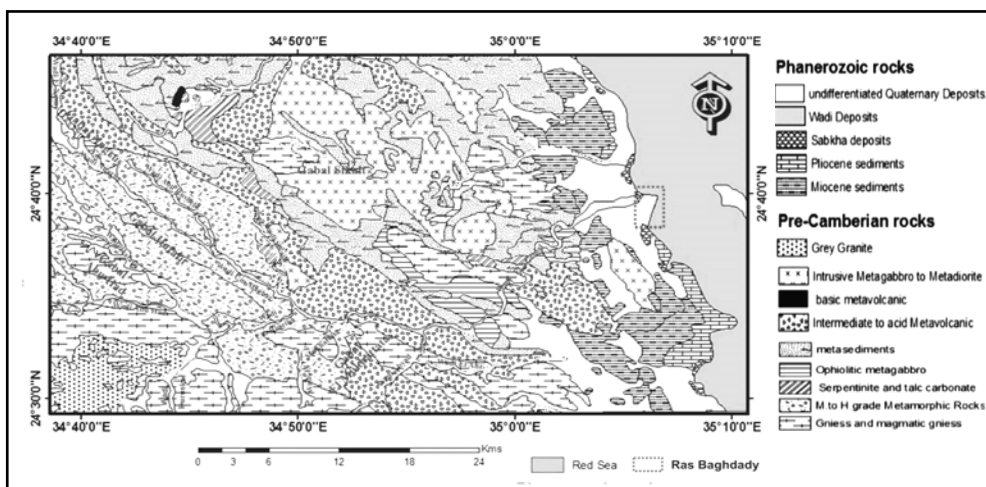

Fig. (3): Geologic map of Wadi El Gemal District (modified by the present authors after Conoco, 1987).

The coastal plain sediments are sporadically distributed from Suez Gulf toward the southern part of the Red Sea coast along the shore line and can be summarized as follow; the beach sediments along the eastern side of the Gulf of Suez, the coastal plain sediment in the area from Hurghada in the north to El Qusier in the south, beach sands at Ras Manazel area which lies south Ras Banas and in delta of Wadi Diit, El Hebal sand dunes, beach and dune black sand at Mersa Shallal and Mersa El Kad near Abu Ramad district. These deposits were mineralogically and geochemically studied by Dabbour et al., (1999), Ramadan and Hoda, (1999), Yousria and El Gohary, (2005), El Kammar et al, (2007), El Hadary,(2008), Ibrahim et al, (2009), Abu Halawa et al, (2010) and El Afandy et al., (2011). In this respect, El Hadary (2008) investigated Wadi El Gemal beach sediments, and concluded that, the heavy minerals were represented by amphiboles, pyroxenes, epidot, kyanite, sturolite, zircon, rutile, garnet, monazite, sphene, magnetite, hematite, goethite and ilmenite while the light minerals were mainly represented by quartz. Moreover, El Hadary (Op. Cit) recommended that, Wadi El Gemal beach sediments are economically promising but they need more detailed studies.

Methods And Techniques Of Work

A total of 30 bulk samples were collected across three profiles A, B and C in traversal proportional distances appropriated with the shoreline topography and morphology (Fig. 4). The studied samples were gathered at constant intervals from digging boreholes using hand auger sampler at 2 m depth (Fig. 5). Five kilograms bulk samples, composed mainly of grey loose sands with little shell fragments and pebbles. Each collected bulk sample was packed and subjected to sun drying then to quartering using the Johns Splitter to obtain representative sample.
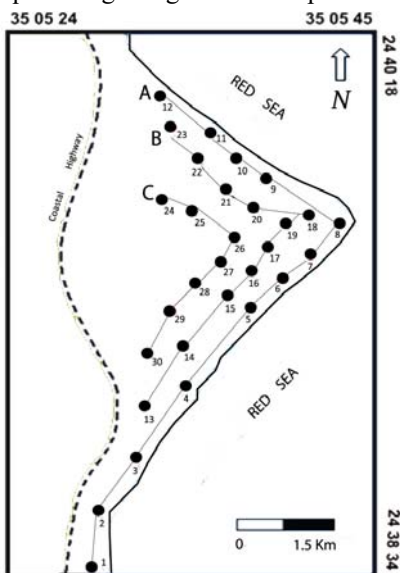

Fig. 4: Sketch map shows samples sites of Ras Baghdady area. A-profile (S.No.1-12), B-profile (S.No.13-23), C-profile (S.No.24-30).
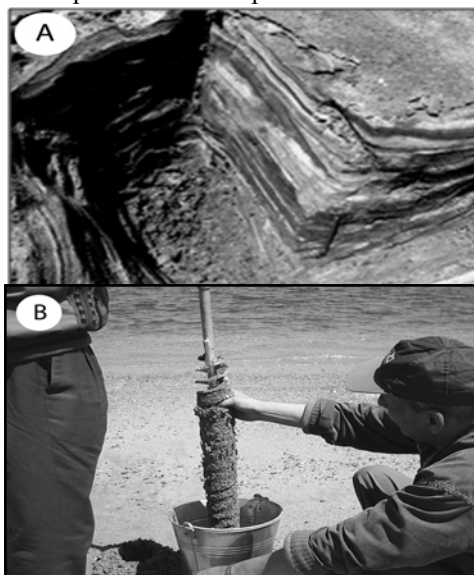
Fig.5: A – Internal structure of Ras Baghdady beach showing regular laminae of heavy minerals (black) alternating with low heavy minerals content (light colored). B – Photograph shows hand auger used for sampling.

Each representative sample was soaked in water and treated with a mixture of hydrochloric acid and stannous chloride (Milner, 1962) to disaggregate and to ensure cleaning of the grains from any coating of carbonates and/or oxides, or even oxyhydroxides (Fig. 6). Further, mechanical analyses were carried out using the conventional sieving method with screen placed at one-phi interval with aid of set of ASTM sieves of 20, 40, 60, 80, 200 and < 200 meshes. Hundred grams of each treated sample sieved in Ro-tap shaker for 15 minutes (Carver, 1971). It was obviously that, the weight percentage of the obtained fractions did not show significant differences within the three profiles (A, B and C). Consequently, the different grain sizes contents can arrange from the highest to the lowest as follow; 0.25-0.125 mm (10-60%), 0.5-0.25 mm (<10 to 20%), and 0.125-0.063 mm (<5 to 10%). Moreover, less than 1% to 10% are randomly distributed between < 0.063 and 1-0.5 mm grain size fractions.

For mineralogical investigations and to reveal the economic potential of the studied beach black sand deposits at the studied locality, all the grain size fractions were preliminarily examined using intermediate power lens to determine the most promising fraction. It has been founded that, the total heavy minerals content of the very fine sand size (0.063–0.125 mm) was nearly equal to that of the fine sand size (0.125–0.25 mm). Meanwhile, the very fine sand size contains the most representative assemblages of the different heavy mineral groups and contains numerous economic mineral species while the fine sand size fraction (0.25-0.125 mm) is mainly composed of green silicate minerals.

About 600 grams of very fine sand size fraction were subjected to wet gravity concentration using the industrial full size Wilfley Shaking table to get high recovery of the economic minerals those have been weighed to be 60 grams of pure heavy minerals. The tabled concentrate sample was quartered and around 30 gm representative sample were subjected to magnetic fractionation by lift-type magnet separator, whereas 6 magnetic and non-magnetic fractions were separated under the following conditions; air gap of 2 mm, feeding rate 10 kg/hour, rotor speed 140 r.p.m. and slope of splitter at 25° between magnetic and non-magnetic fractions (Abu Halawa, 2005). In order to facilitate mineral identification, the separated sub-samples were mineralogically studied and picked using binocular stereomicroscope.

X-ray diffraction analyses were carried out to assess the variability of mineralogical compositions of Fe-Ti bearing phases, to reveal the type of the exsolved titaniferous minerals associated, and to study the alteration products. X-ray diffraction analyses were carried out using the Phillips type (1010-62) with Cu tube and Ni filter.

The Environmental Scanning Electron Microscope (ESEM) technique was used for mineral grains examination using back scattered electron (BSE) image. The ESEM is equipped with energy dispersive X-ray spectrometer (EDX) for chemical analyses for both picked detrital transparent mineral grains and mounted opaque minerals in polished sections. Although, the obtained chemical data by EDX technique are semi-quantitative, the technique can be useful in identification of inclusions in grains, surface texture, staining, ex-solution textures and chemical variations of mineral varieties. Therefore, ESEM technique is further supported to the XRD techniques. The obtained results using the above-mentioned techniques have

increased our knowledge of heavy mineral characteristics and have provided a better understanding of their behaviors during transportation, and deposition as well as post-deposition circumstances. On the other hand, these techniques are important to predict the potential for recovering the Fe-Ti ore minerals and the behavior of these ores during processing. Besides, it is necessary to identify trace elements that have bearing on recovery of the elements and on the purity of refined metals. The XRD and SEM analytical techniques that applied for the various economic heavy mineral species; were carried out at the Laboratories of the Egyptian Nuclear Materials Authority.

Results And Discussion

The total heavy mineral fractions (Fig. 7A) separated into five magnetic sub-fractions. These magnetic sub-fractions are individually weighted and their values are given in table (1) to be used in computation of the economic mineral contents. About 1000 particles from each magnetic fraction were identified and counted using the binocular stereomicroscope. The weight percent (wt. %) of each mineral in each fraction was recalculated then its content in each original sample was determined. The relative average contents of the heavy minerals assemblage in these sub-fractions are shown in table (2) and figure (7 B & C).

The detailed mineralogical compositions of the separated magnetic and non-magnetic sub-fractions are as follows:

1. Magnetite fraction (0.08 amp.): This fraction is composed essentially of magnetite and green silicates. Magnetite content reaching about 71.43% of the total fraction ranges from 0.06 Wt% to 4.91 wt.% with 1.25 wt.% average. The average of second component green silicate reaches an average content of about 0.5 wt.% forming about 28.57 % of the total fraction.

2. Ilmenite-I fraction (0.6 amp.): Ilmenite fraction forming 9.52 % of the total fraction, is composed essentially of ilmenite, garnet, goethite and green silicates. Ilmenite content varies in this fraction from 0.71 wt.% to 11.7 wt.% of average 3.12 wt.% content. Unfortunately, both of goethite and garnet contents constitute only 1.68 wt.% and 1.09 wt.% respectively. Moreover, the recorded paramagnetic green silicate minerals (pyroxenes, amphiboles and epidote) content is around 28.79 wt. % forming 87.85 % of the total fraction.

3. Ilmenite-II fraction (1.0 amp.) is composed essentially of ilmenite, goethite and garnet with low contents matching 2.09 %, 0.9 % and 0.5% of the total fraction, respectively. On contrary, green silicate minerals content records up to 96.51 %. Furthermore, the total fraction is somewhat similar to that obtained at 1.5 amp. by the Frantz Isodynmic magnetic separator under the previously mentioned conditions in ilmenite I fraction.

4. Ilmenite-III fraction (2.0 amp.) is composed essentially of ilmenite and garnet and green silicates. Both of ilmenite and garnet record 1.66 % and 3.13 % of the total fraction respectively. However, the green silicate mineral assemblage increase reaches 95.21 % of the total fraction.

5. The non-magnetic fraction (2.0 amp.) is composed essentially of zircon (13.11 %), sphene (9.17 %), and rutile (7.54 %), in addition to trace amount of non-magnetic

leucoxene (0.07 %) and other rock forming minerals as amphiboles and pyroxenes (70.12 %). This fraction is equivalent to the 1.5 amp. non-magnetic fraction of the Frantz Isodynamic magnetic separator under the given conditions.

Table (1): Weights of magnetic sub-fractions and total heavy fractions (in grams) of the grain size (0.125-0.063 mm).

S. No.	(ρ_1) 0.08 A	(ρ_2) 0.6 A	(ρ_3) 1.0 A	(ρ_4) 2.0 A	(ρ_5) 2.0 A *N/Mag	(P) Total Heavy Fraction
1	0.12	1.54	1.59	0.32	0.08	3.65
2	0.16	2.27	2.34	0.47	0.12	5.37
3	0.21	2.78	2.49	1.45	0.19	7.12
4	0.16	1.83	2.33	0.53	0.31	5.16
5	0.01	0.45	0.96	0.15	0.04	1.60
6	0.001	0.22	0.66	0.09	0.02	1.00
7	0.001	0.35	1.25	0.20	0.04	1.84
8	0.04	0.26	0.91	0.29	0.03	1.52
9	0.08	1.39	2.36	0.36	0.11	4.30
10	0.05	1.71	1.57	0.33	0.10	3.77
11	0.20	1.13	1.09	0.34	0.07	2.84
12	0.03	0.43	0.61	0.09	0.02	1.18
13	0.13	1.42	2.81	0.48	0.28	5.13
14	0.10	1.22	1.40	0.36	0.11	3.19
15	0.01	1.03	1.53	0.19	0.11	2.88
16	0.01	1.96	2.08	0.39	0.20	4.64
17	0.01	1.01	1.71	0.31	0.11	3.16
18	0.01	1.38	2.26	0.27	0.08	4.00
19	0.03	0.54	1.18	0.13	0.03	1.91
20	0.004	0.13	0.47	0.071	0.014	0.69
21	0.02	0.47	1.65	0.25	0.05	2.43
22	0.10	0.60	1.13	0.16	0.06	2.04
23	0.04	0.52	0.67	0.27	0.06	1.56
24	0.03	2.50	2.53	0.33	0.25	5.65
25	0.00	0.88	1.82	0.24	0.06	3.01
26	0.01	0.37	0.91	0.22	0.04	1.55
27	0.04	0.92	1.67	0.27	0.08	2.98
28	0.02	0.82	1.68	0.28	0.08	2.88
29	0.03	1.28	1.58	0.59	0.23	3.72
30	0.15	3.40	2.12	0.40	0.35	6.42
Average	0.06	1.10	1.51	0.31	0.11	3.24

*N/Mag: Non-magnetic fraction.

Table (2): Averages relative frequencies (wt. %) of the heavy minerals assemblage in magnetic sub-fractions of the size range (0.125 -0.063 mm, samples number = 30).

Magnetic Subfractions	Items Minerals	Min. Wt %	Max. Wt %	Average Wt %
0.08 A	Magnetite	0.06	4.91	1.25
	Green Silicates	0.02	2.35	0.50
0.6 A	Ilmenite	0.71	11.70	3.12
	Garnet	0.00	1.68	0.37
	Goethite	0.20	1.09	0.49
	Green Silicates	15.44	44.67	28.79
1.0 A	Ilmenite	0.28	3.90	1.09
	Garnet	0.00	1.47	0.26
	Goethite	0.00	0.96	0.47
	Green Silicates	31.25	65.79	50.38
2.0 A Magnetic	Ilmenite	0.00	1.14	0.17
	Garnet	0.00	8.72	0.32
	Green Silicates	0.03	20.37	9.74
2.0 A Non-magnetic	Zircon	0.03	1.86	0.40
	Rutile	0.03	1.01	0.23
	Sphene	0.00	1.50	0.28
	Leucoxene	0.00	0.02	0.002
	Others	0.00	4.22	2.14
				100

Characteristics of the picked heavy minerals

The mineralogical studies are concerned with the comparative mechanical, physical and chemical properties of economic heavy mineral grains which may contribute further information regarding their utilization. Mineralogical investigations aim to identify the various species of the economic heavy minerals and examination of their physical external features including grain morphology, color, and surface texture, besides, examination of internal features such as inclusions, ex-solution textures and dissolution textures. These features may be evident the chemical and mechanical weathering, transportation agent, depositional, post-depositional and digenetic conditions. Hereunder, the detailed physical and chemical properties of the different heavy mineral kinds detected at the studied locality are given.

The physical features of the detected heavy minerals:

The detrital Fe-Ti oxide minerals include opaque ilmenite, magnetite and goethite as well as translucent rutile. These form the most abundant constituents reaching ~ 81% of the total economic minerals in Ras Baghdady beach sands.
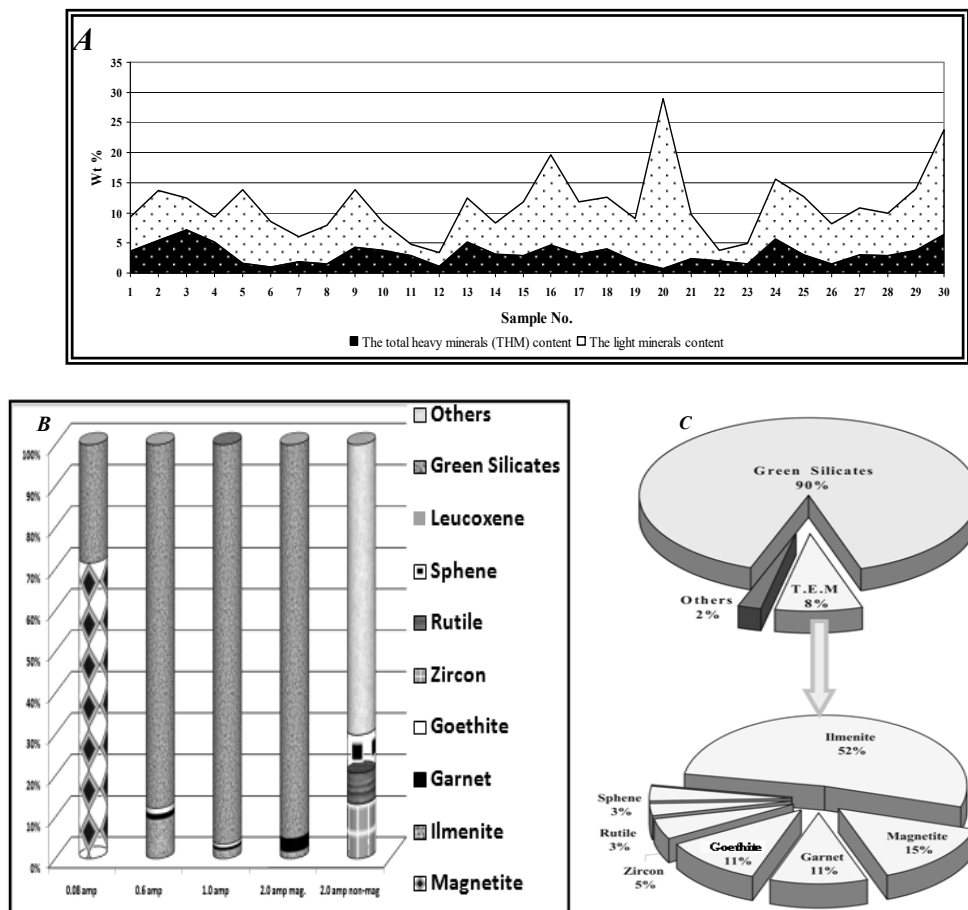
Fig. (7): (A) The total heavy mineral content in the studied size fraction (0.125-0.063 mm);
   (B) Averages relative frequencies (wt.%) of the heavy minerals assemblage in magnetic and non-magnetic sub-fractions of the size range (0.125-0.063 mm);
   (C) Pie-diagrams shows; content of the total economic minerals (T.E.M) % relative to the total heavy minerals% and relative contents of individual economic minerals % in the grain size interval (0.125-0.063 mm) of Ras Baghdady beach sands.

Ilmenite (FeTiO₃):

   Ilmenite represents the major mineral constituent (~52%) among the total mineral assemblages of economic interest in the studied very fine sand class (0.125-0.063 mm). The present ilmenite was fractionated magnetically, based on its magnetic susceptibility, by the lift-type magnet separator into three classes; (I), (II) and (III) at 0.15, 0.3 and 0.45 amp., respectively. Under binocular stereomicroscope, ilmenite grains appear to be angular to sub-angular due to the short-distance transportation and favoring low-energy deposition. Furthermore, the conchoidal fracturing recorded in

the grains may be due to grain/grain collision during transport. Almost, all the grains in these classes appear to be mainly deep blue to black in color with metallic to sub-metallic luster. Few grains depicted yellowish brown to yellowish white stains that probably due to alteration. These may suggest the predominance of the fresh ilmenite in early stage of alteration (Fig. 8A & B and C). Some traces of yellowish white color leucoxenated ilmenite grains are also observed in the studied ilmenite fractions (Fig. 8D).
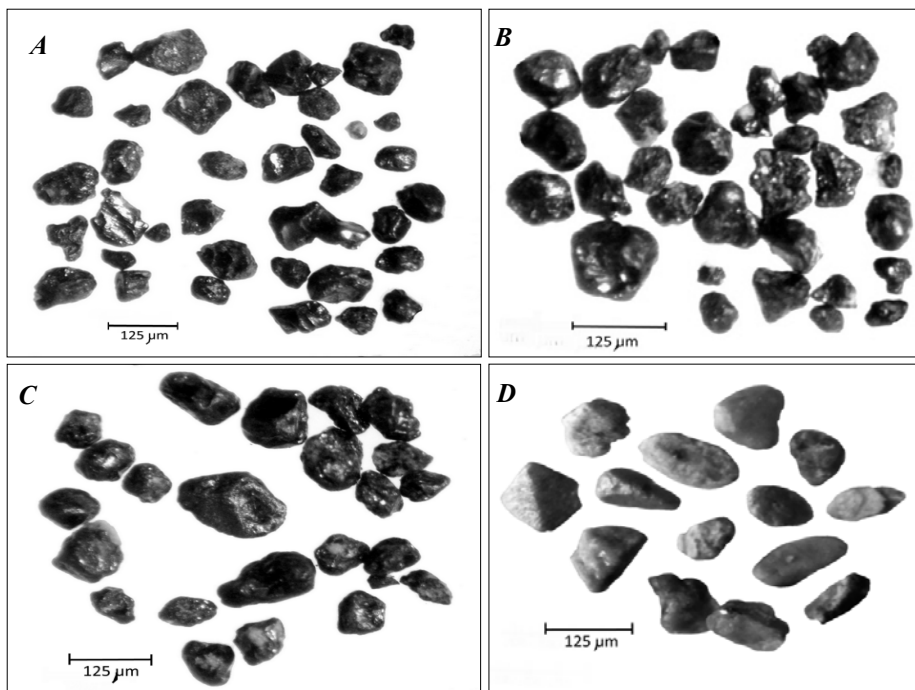

Fig. (8): (A) Photomicrographs show;(A) Ilmenite class-I separated at 0.15 amp.; **(B)** Ilmenite class-II separated at 0.3 amp.;
(C) Ilmenite class-III separated at 0.45 amp.; **(D)** Leucoxenated ilmenite grain separated from the beach sand of Ras Baghdady area, Red Sea coast, Egypt.

Moreover, the X-ray diffraction patterns depict sharp and prominent peaks of homogeneous pure ilmenite mineral that persist only in the fraction of ilmenite class (III) separated at 0.45 ampere current. Meanwhile, sharp intensity peaks of rutile and hematite (Figs. 10 & 11) are obviously depicted in the fractions of ilmenite classes I and II indicating in situ decomposition of ilmenite (for more details see Suresh Babu, et al., 1994). The difference in the degree of ilmenite alteration in various heavy mineral placer deposits implies differential weathering due to age differences and/or in situ and multistage alteration of ilmenite (Hugo and Cornell 1991) and also due to different weathering environments.
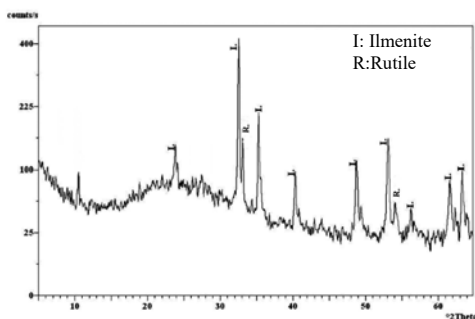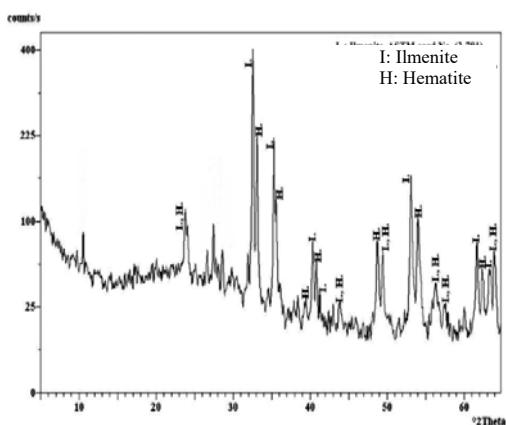
dA°	I/Io	Ilmenite A S T M (3-0781)		Rutile A S T M (21-1276)	
		dA°	I/Io	dA°	I/Io
3.37	20	3.73	50		
2.75	100	2.74	100		
2.70	27				
2.54	72	2.54	85		
2.23	19	2.23	70		
1.87	26	1.86	85		
1.72	40	1.72	100		
1.69	16			1.68	60
1.63	7	1.63	50	1.62	20
1.56	17	1.50	85		
1.47	27	1.47	85	1.45	10

Fig. (9): X-ray diffractograph (XRD) of leucoxenated ilmenite class-III with its ASTM reference values.
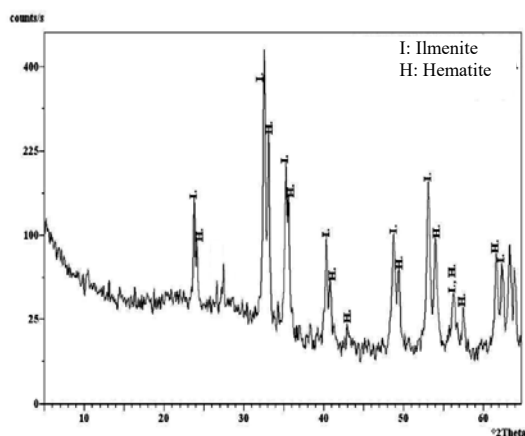
dA°	I/Io	Ilmenite A S T M (3-0781)		Hematite A S T M (13-0534)	
		dA°	I/Io	dA°	I/Io
3.73	25	3.73	50		
3.69	13			3.66	25
2.75	100	2.74	100		
2.70	65			2.69	100
2.54	42	2.54	85		
2.52	31			2.51	50
2.23	19	2.23	70		
2.21	10			2.201	30
2.09	2			2.07	2
1.87	19	1.86	85		
1.84	16			1.838	40
1.72	37	1.72	100		
1.76	20			1.69	60
1.63	8	1.63	50		
1.66	5			1.634	4
1.65	14	1.50	85	1.596	16
1.49	15			1.484	35
1.47	18	1.47	85		

Fig. (10): X-ray diffractograph (XRD) of weakly magnetic ilmenite class-II with its ASTM reference values.

dA°	I/Io	Ilmenite A S T M (3-0781)		Hematite A S T M (13-0534)	
		dA°	I/Io	dA°	I/Io
3.14	19	2.737	30	3.66	25
2.75	100	2.754	100		
2.70	55			2.69	100
2.54	60	2.544	70		
2.52	34			2.51	50
2.28	3			2.285	2
2.23	15	2.237	30		
2.21	13			2.201	30
2.19	10	2.1772	2		
2.06	3	2.1032	2	2.07	2
1.87	18	1.8683	40		
1.84	14	1.8309	1	1.838	40
1.72	51	1.7261	55		
1.70	24			1.69	60
1.63	7	1.6354	9	1.634	4
1.60	3	1.6206	3	1.596	16
1.50	10	1.5053	30		
1.49	10			1.484	35
1.47	9	1.4686	35		
1.46	17	1.4342	1	1.452	35

Fig. (11): X-ray diffractograph (XRD) of weakly magnetic ilmenite class-I with its ASTM reference values.

Rutile (TiO₂):

Rutile that occurs either as euhedral vertically striated tetragonal prisms with rounded pyramidal terminations or as furrowed prismatic faces, constitutes about 0.23 wt.% of the original raw sand (0.125- 0.063 mm) reaching 3 % of the total economic minerals of Ras Baghdady beach sands. Rutile is quite non-magnetic mineral, hence, it separated in the non-magnetic fraction at 2.0 amp. The recorded rutile grains are translucent with resinous luster, meanwhile, some reddish brown and black varieties with numerous shapes are also recorded. Because of extremely high refractive indices, a thick black halo surrounds the grains (fig. 12 A). Some rutile grains show elbow twinning and heart-like shapes. Moreover, elongated, tablet-like shape, ovate, triangular and irregular shape of rutile grains are also recorded (Fig. 12 B). The X-ray diffraction patterns of the black rutile reveal that, the peaks intensity shows little and short peaks of minor ilmenite constituents associated with abundant and prominent rutile peaks (Fig. 13). Meanwhile, the XRD patterns of the reddish brown variety illustrate the predominant peaks intensity of pure rutile (Fig. 14).
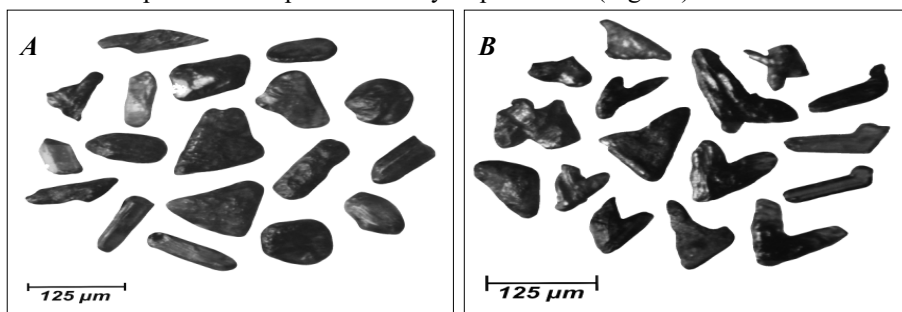

Fig. (12): Photomicrographs showing black and reddish brown varieties of rutile crystals in the non-magnetic fraction separated at 2.0 amp.; (A) elongated, ovatetriangular and tablet-like shaped grains depicting a thick black halo; (B) irregular, elbow twinning (at right) and heart-like shaped grains.
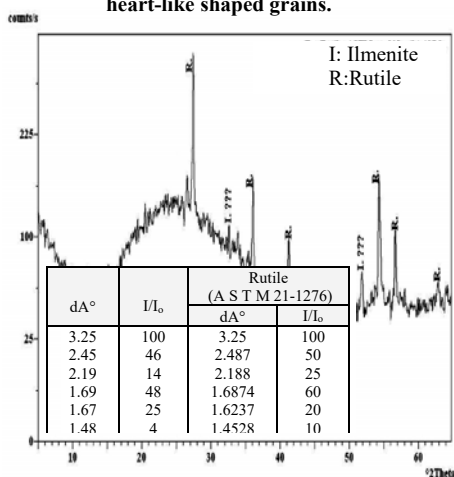

dA°	I/I_o	Rutile (A S T M 21-1276)	
		dA°	I/I_o
3.25	100	3.25	100
2.45	46	2.487	50
2.19	14	2.188	25
1.69	48	1.6874	60
1.67	25	1.6237	20
1.48	4	1.4528	10

Fig. (13): X-ray diffractograph (XRD) of the black rutile in the non-magnetic fraction II with its ASTM reference values.

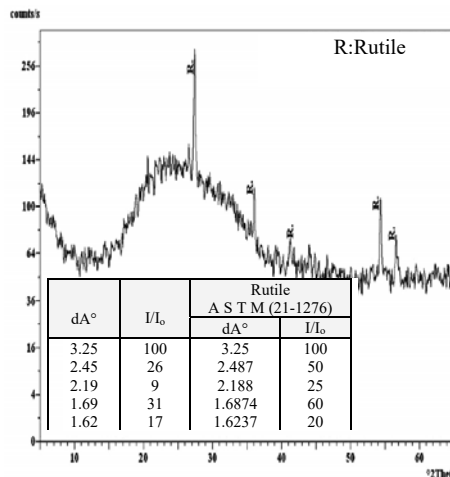| dA°	I/I_o	Rutile A S T M (21-1276)	
		dA°	I/I_o
3.25	100	3.25	100
2.45	26	2.487	50
2.19	9	2.188	25
1.69	31	1.6874	60
1.62	17	1.6237	20

Fig. (14): X-ray diffractograph (XRD) of the reddish brown rutile in the non-magnetic fraction with its ASTM reference values.

Magnetite (Fe₃O₄):

Magnetite as a second abundant economic mineral constitutes about 15% of the total economic minerals. Frequency of magnetite in the studied beach sands ranges from 0.06 wt.% to 4.91 wt.% with 1.25 wt.%. in average. Magnetite is a black medium to fine grained with metallic luster and exhibits botryoidal or cluster aggregates of angular to sub-angular grains. Some magnetite grains show adhering fragments of transparent to translucent gangue silicate minerals (Fig. 15). The presence of some reddish brown magnetite grains observed under binocular stereo-microscope is attributed to effective alteration processes (i.e. martitization, hematitization and maghamitization) affecting the fresh black magnetite grains as well as presence of the exsolved titaniferous mineral (Hammoud, 1966 & 1973). In this respect, Mucke and Raphael (2005) stated that the change in redox reactions (i.e. oxidizing or reducing fluids solutions) produced pseudomorphic replacements known as martitization (replacement of magnetite by hematite due to oxidation). On the other hand, replacement of hematite by magnetite due to simple addition of Fe^{2+} atoms under basic conditions is restricted to unlithified sediments only. Moreover, X-ray diffraction analysis of magnetite fraction points to presence of high peaks intensity of the associated hematite and ilmenite minerals within this fraction (Fig.16).
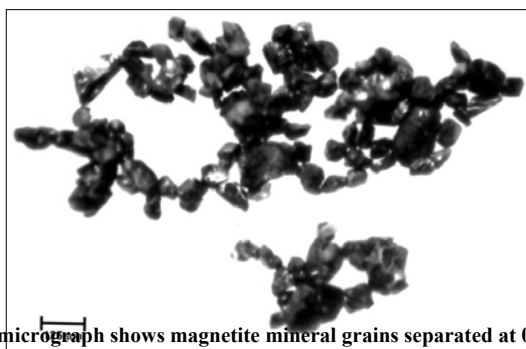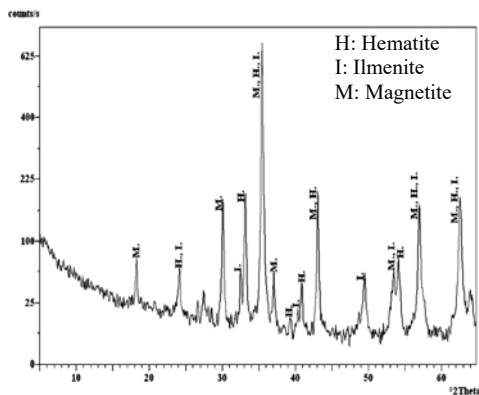

Fig. (15): Photomicrograph shows magnetite mineral grains separated at 0.08 amp.

dA°	I/I₀	Magnetite A S T M (19-0629)		Hematite A S T M (13-0534)		Ilmenite A S T M (3-0781)	
		dA°	I/I₀	dA°	I/I₀	dA°	I/I₀
4.85	8	4.85	8				
3.68	7			3.66	25	3.73	50
2.96	25	2.967	30				
2.75	9					2.74	100
2.70	29			2.69	100		
2.53	100	2.532	100	2.51	50	2.54	85
2.42	10	2.424	8				
2.29	0.9			2.285	2		
2.23	1.8					2.23	70
2.20	4			2.201	30		
2.09	28	2.099	20	2.07	2		
1.84	7					1.86	85
1.71	8	1.715	10			1.72	100
1.69	10			1.69	60		
1.62	28	1.616	30	1.596	16	1.63	50
1.48	31	1.484	40	1.484	35	1.47	85

H: Hematite
I: Ilmenite
M: Magnetite

Fig. (16): X-ray diffractograph (XRD) of magnetite with its ASTM reference values.

2.4- Goethite [α-Fe⁺³O (OH)]:

2.4- Goethite [α-Fe^{+3}O (OH)]:

Goethite contents in Ras Baghdady beach sands range between 1.15 wt.% to 13.88 wt.% to reach about 11% of the total economic minerals with an average of 4.38 wt.%. Although, goethite contains theoretically high iron content (62.9 %), goethite often very weakly or non-magnetic mineral. Hence, it separated in the non-magnetic fraction at 0.6 ampere current. Goethite grains are blackish brown elongated prismatic crystals with submetallic and dull luster as well as uneven fractures (Fig. 17A). Some traces of deep brown regular pyritohedral cubes of goethite crystals are also recorded in the studied beach sands (Fig. 17B) due to short distance transportation.
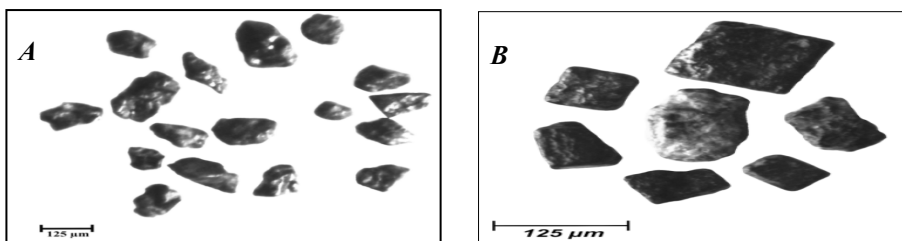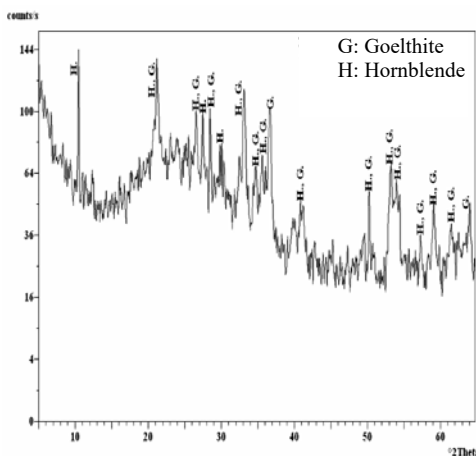

Fig. (17): Photomicrographs show; (A) goethite crystals in the non-magnetic fraction separated at 0.6 amp.; (B) pyrite cube in the non-magnetic fraction separated at 0.6 amp.

dA°	I/I$_o$	Hornblende ASTM (20-0481) dA°	Hornblende ASTM (20-0481) I/I$_o$	Goethite ASTM (17-0536) dA°	Goethite ASTM (17-0536) I/I$_o$
8.42	100	8.40	100		
4.19	48	4.19	14	4.18	100
3.35	25	3.39	10	3.38	10
3.24	29	3.26	20		
3.13	35	3.10	70		
2.98	15	2.939	10		
2.70	53	2.697	20	2.69	30
2.59	17	2.587	8	2.58	8
2.52	25	2.537	6	2.52	4
2.45	55			2.452	25
2.20	11	2.21	<1	2.192	20
1.82	46	1.798	2	1.799	8
1.72	33	1.737	2	1.721	20
1.69	21	1.681	2	1.694	10
1.56	19	1.555	2	1.564	16
1.51	12	1.524	2	1.509	10
1.45	18			1.453	10

G: Goelthite
H: Hornblende

Fig. (18): X-ray diffractograph (XRD) of goethite in the non-magnetic fraction with it ASTM reference values.

Garnet [X₃Y₂(SiO₄)₃]:

Garnet [X$_3$Y$_2$(SiO$_4$)$_3$]:

The recorded garnet forms about 11% of the total economic heavy minerals with 0.95 wt.%. average content in separated sand size 0.125-0.063 mm. The separated vitreous luster garnet grains reflect pink to brownish red color occasionally with a violet tint and occur as euhedral crystals, sharp irregular fragments, and sub-rounded to rounded grains. Furthermore, uneven or conchoidal fractures are also exhibited

(Fig. 19). The XRD pattern confirms the predominance of spessartine garnet $[Mn_3Al_2(SiO_4)_3]$ in the magnetic fraction separated at 0.6 amp. in the studied black sands (Fig. 20).
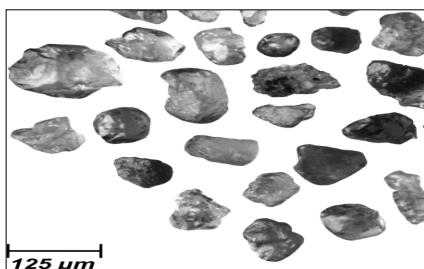

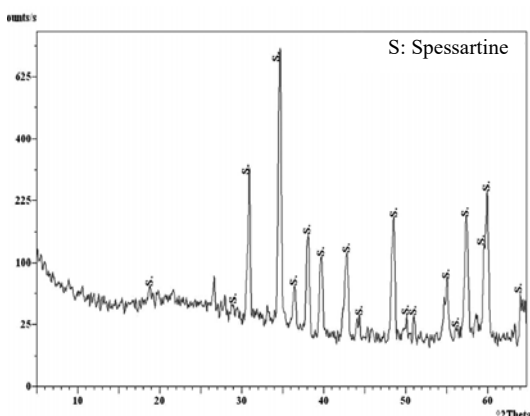**Fig. (19): Photomicrograph shows pink garnet in the magnetic fraction separated at 0.6 amp.**

Fig. (20): X-ray diffractograph (XRD) of spessartine garnet with ASTM reference values.

dA°	I/I$_o$	Spessartine A S T M (10-0354)	
		dA°	I/I$_o$
4.70	2	4.76	6
3.09	1	3.10	8
2.89	50	2.91	25
2.58	100	2.60	100
2.46	5	2.46	10
2.36	18	2.37	16
2.26	15	2.28	10
2.11	14	2.13	16
2.05	2	2.06	6
1.87	23	1.886	20
1.82	1	1.836	2
1.79	5	1.797	2
1.67	10	1.681	20
1.64	1	1.65	6
1.60	26	1.614	30
1.57	2	1.586	6
1.54	41	1.557	40
1.45	6	1.456	16

Zircon (ZrSiO$_4$):

Grain count data points to presence of ~ 0.4 wt.% zircon in the studied bulk sample to form 5% of the total economic minerals assemblage. In general, the majority of zircon crystals are colorless with vitreous luster, and occasionally with internal shades of reddish brown color probably due to iron oxide stains. The detected colorless zircon grains occur either as elongate sub-rounded to rounded grains or as idiomorphic prismatic crystals with rounded terminations (Fig. 21A). Meanwhile, another zircon varieties that reflect orange, rosy, brown and deep red color grains occur as oval, needle, barrel and elongated crystals (Fig. 21B). It is interesting to notice that the malacon zircon with dusky dark gray in color, is well preserved as idiomorphic bipyramidal crystals (Fig. 21C). This phenomenon may attribute to the ultra-stability of malacon zircon variety (idiomorphic bipyramidal crystals) over the other varieties. Besides, metamictic and zoned zircon grains occur as brittle or fractured crystals that probably due to radioactive decay (Fig. 21D).
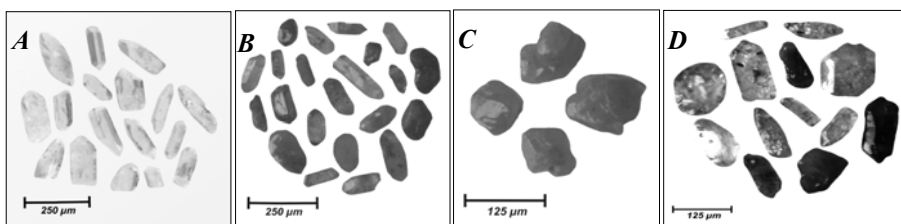
Fig. (21): Photomicrographs show; (A) colorless elongate grains and prismatic zircon crystals with rounded terminations; (B) oval, elongate, sub-rounded and rounded colored zircon crystals of orange, rosy, brown and deep red varieties; (C) idiomorphic bipyramidal malacon zircon crystals with overgrowth; and (D) brittle or fractured zircon grains with black and brown metamict zircon.

Some zircon grains exhibit twinning (Fig. 22A), while another grains have commonly radiated fractures from the center, that could be caused by inclusions or by radioactive decay (Fig. 22B). In this respect, Hutton (1950) attributed this phenomenon to zircon radioactivity. Moreover, the common crystalline inclusions according to Hammoud, (1966) are monazite, hematite, magnetite, quartz, apatite and rutile. Another twined zircon grains are epitaxially overgrown by a later generation of zircon aggregates developed on one part of the grain (Fig. 22C).
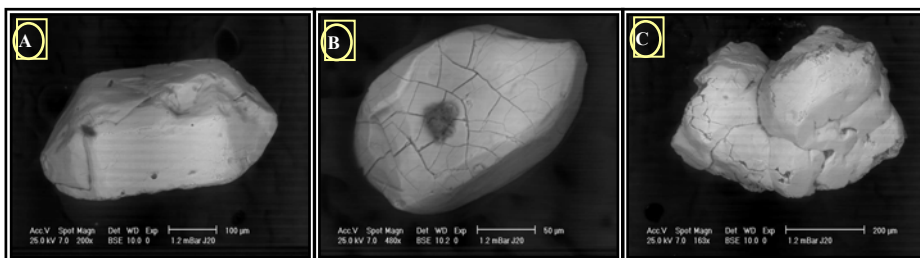

Fig. (22): Back scattered electron (BSE) images show; (A) twinned zircon crystal; (B) zircon grain with fractures radiated from central inclusion; and (C) composite grain of zircon aggregates.

The X-ray diffraction patterns of zircon concentrate indicate presence of fluorapatite and hematite within the colorless zircon sample (Fig. 23), which can be explained by presence of these minerals as inclusions. Meantime, apatite can associate zircon due to similarity in several morphological and mineralogical features. Moreover, hematite may also be present as stains in the cracks and fractures of zircon grains. Furthermore, The peaks intensity of the colored zircon sample reveal presence of titanite as inclusions within zircon grains (Fig. 24).

Sphene (titanite; [CaTi [SiO4] (O, OH, F)]:

Both of sphene and rutile exhibit the lowest abundant content (~ 3%) among the total economic minerals. Meanwhile, sphene shows higher average content (~ 0.28 wt.%) than rutile (~ 0.23 wt. %) in the studied sand class (125-63 µm). Most of titanite grains were recovered in the non-magnetic fraction at 2.0 amp., and possesses honey yellow to light brown color with resinous luster. Further, sphene outline is surrounded by a dark rim as a result of high refractive index and differential absorption of light that controlled by presence of impurities. Sphene irregular grains occur as rounded, equant,

tabular and/or sphenoidal crystals shape with a tendency to sphericity. Besides, surface etching, facets and etch-pits are also recorded witin the studied grains (Fig. 25). The X-ray diffraction patterns of the concentrated sphene mineral (titanite) depict the predominant peaks intensity of pure sphene mineral with relatively homogeneous phase (Fig. 26 and table, 13).
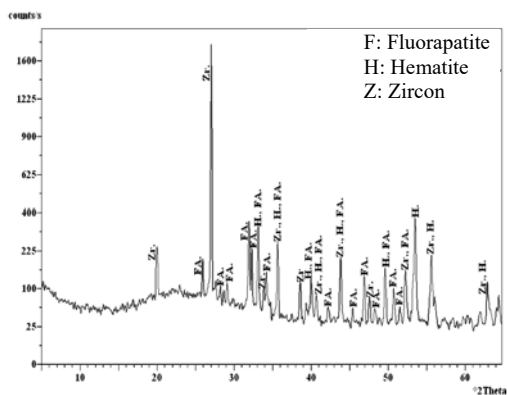

F: Fluorapatite
H: Hematite
Z: Zircon

Fig. (23): X-ray diffractograph (XRD) of colorless zircon in the non-magnetic fraction with ASTM reference values.

dA°	I/I₀	Zircon A S T M (6-0266)		Hematite A S T M (13-0534)		Fluorapatite A S T M (15-0876)	
		dA°	I/I₀	dA°	I/I₀	dA°	I/I₀
4.45	8	4.434	45				
3.34	6					3.442	40
3.36	100	3.302	100				
3.16	3					3.167	14
3.07	2					3.067	18
2.80	18					2.800	100
2.77	8					2.772	55
2.70	15			2.690	100	2.702	60
2.64	3	2.65	8				
2.62	5					2.624	30
2.52	11	2.518	45	2.51	50	2.517	6
2.33	5	2.336	16				
2.29	3			2.285	2	2.289	8
2.25	4					2.250	20
2.22	3	2.217	8	2.201	30	2.218	4
2.14	1					2.140	6
2.06	9	2.066	26	2.070	2	2.061	6
2.00	2					2.028	2
1.94	7					1.937	25
1.91	2	1.908	14				
1.88	1					1.884	14
1.84	7			1.838	40	1.837	30
1.80	4					1.797	16
1.77	2					1.771	14
1.75	6	1.751	12				1.748	14

T. : Titanite, ASTM card No. (11-142).
Zr. : Zircon. ASTM card No. (6-0266).
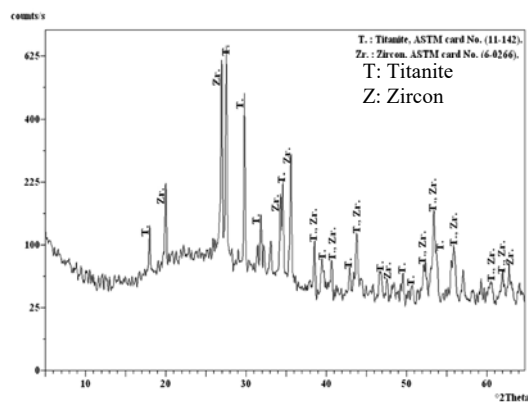
T: Titanite
Z: Zircon

Fig. (24): X-ray diffractograph (XRD) of colored zircon in the non-magnetic fraction with ASTM reference values.

dA°	I/I₀	Titanite A S T M (11-0142)		Zircon A S T M (6-0266)	
		dA°	I/I₀	dA°	I/I₀
4.92	12	4.43	30		
4.43	18			4.43	45
3.30	82			3.30	100
3.24	100	3.233	100		
2.99	75	2.989	90		
2.81	13	2.841	5		
2.61	19			2.65	8
2.59	28	2.595	90		
2.52	43			2.518	45
2.33	12	2.362	5	2.336	10
2.28	5	2.273	30		
2.22	10	2.225	5	2.217	8
2.11	4	2.101	20		
2.06	16	2.058	40	2.066	20
1.94	3	1.945	10		
1.91	2			1.908	14
1.84	4	1.848	5		
1.80	2	1.802	10		
1.75	4	1.741	20	1.751	12
1.72	5	1.725	10	1.712	40
1.71	17	1.705	30		
1.64	13	1.643	40	1.651	14
1.53	2	1.527	10	1.547	4
1.50	4	1.494	40	1.495	4
1.48	6			1.477	8

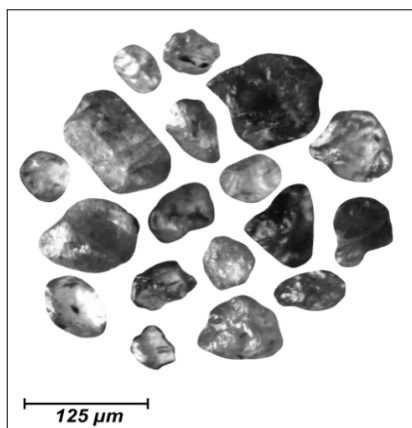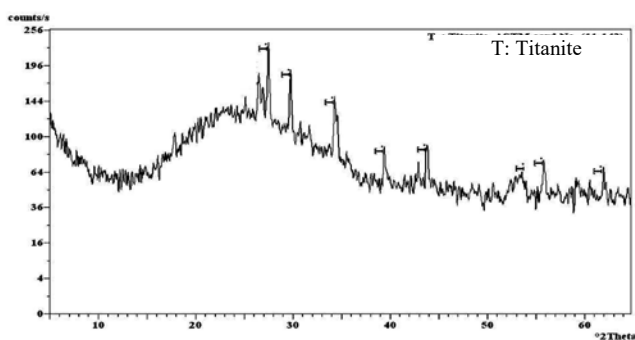Fig. (25): Photomicrograph shows sphene mineral in the non-magnetic fraction separated at 2.0 amp.

dA°	I/Iₒ	Sphene A S T M (11-0142)	
		dA°	I/Iₒ
3.24	100	3.233	100
2.99	82	2.989	90
2.61	62	1.595	90
2.29	31	2.273	30
2.06	36	2.058	40
1.71	14	1.703	30
1.64	26	1.643	40
1.50	30	1.494	40

Fig. (26): X-ray diffractograph (XRD) of sphene (titanite) in the non-magnetic fraction with ASTM reference values.

Radioactive, rare earth elements (REE) bearing minerals and gemstones:
4.1- Monazite: (Ce, La, Nd, Th) PO₄

Monazite is recorded in the studied beach sands as a minor constituent. The monazite grains occur as largely translucent in different hues of yellow; from clear deep canary and lemon yellow, to shades of apple green with resinous luster. Many grains are stained in places with varying amounts of penetrative impurities probably iron oxides. Monazite mineral varies from rounded to sub-rounded crystals with different shapes such as oval, barrel and sometimes tabular. Furthermore, pits and groves are common on its surfaces (Fig. 27). The monazite semi-quantitative chemical analysis shows that, it contains up to 18.3% P_2O_5 and up to 61.2% light rare earth elements (i.e. Ce, La and Nd). Monazite is high in Th and U contents (~ 6.70% and ~ 5.4%, respectively). The most important characteristic features of the picked monazite are the high content of Nd (17. 3%) and Sm (4.37%) as well as the low content of La (9.63%).
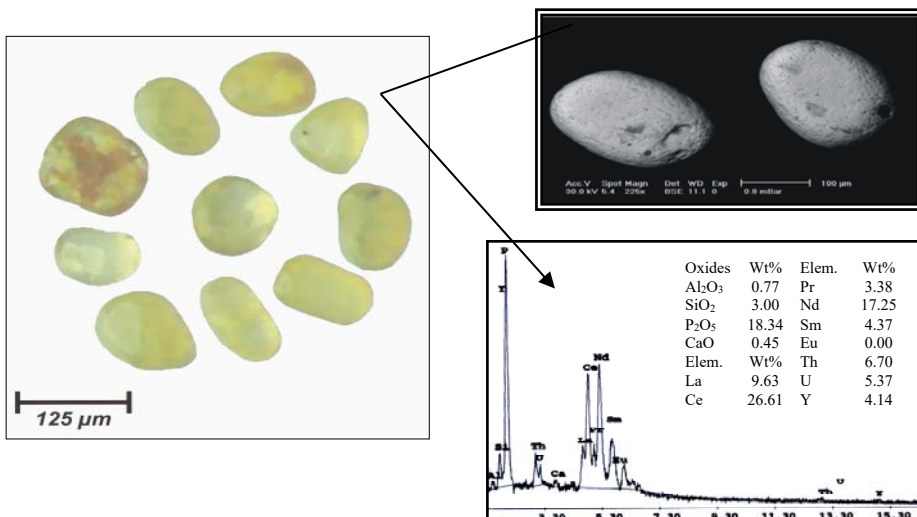
Oxides	Wt%	Elem.	Wt%
Al₂O₃	0.77	Pr	3.38
SiO₂	3.00	Nd	17.25
P₂O₅	18.34	Sm	4.37
CaO	0.45	Eu	0.00
Elem.	Wt%	Th	6.70
La	9.63	U	5.37
Ce	26.61	Y	4.14

Fig. (27): Photomicrograph, BSE image and EDX of monazite separated from beach sands of Ras Baghdady area, Red Sea coast, Egypt.

Uranothorite: (U,Th,Y)SiO₄

Uranothorite is commonly occurred as dark brown grains with a resinous or greasy luster. Although uranothorite is normally non-magnetic but recovered from the weakly magnetic fraction due to its iron content (~ 8.97%). The semi-quantitative EDX analysis of the picked uranothorite grains show that, the average Th, U, Y and Si contents are 40.12%, 11.77%, 11.9 and 10.29%, respectively (Fig. 28).
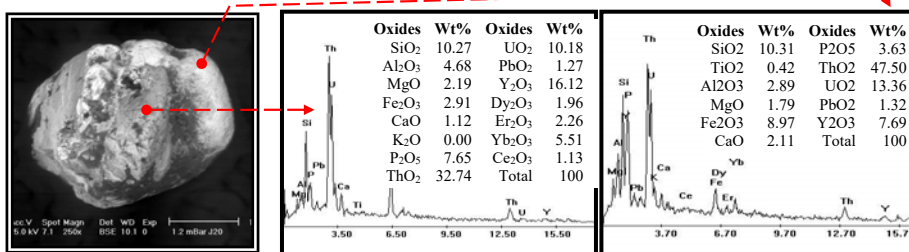

Fig. (28): Backscattered Electron image and EDX of uranothorite separated from beach sands of Ras Baghdady area, Red Sea coast, Egypt.

4.3- Xenotime: (Y, HREE) PO₄

Xenotime occurs as bipyramidal pink to red grains, with a resinous luster. Xenotime was recovered in the moderately magnetic fraction. Semi-quantitative EDX analysis shows that, xenotime contains 25.53% of Y₂O₃ and 29.2% of P₂O₅ (Fig. 29), and contains 4.97% of Yb₂O₃, 4.19% of Nd₂O₃ and 3.46% of Ce₂O₃ as well.
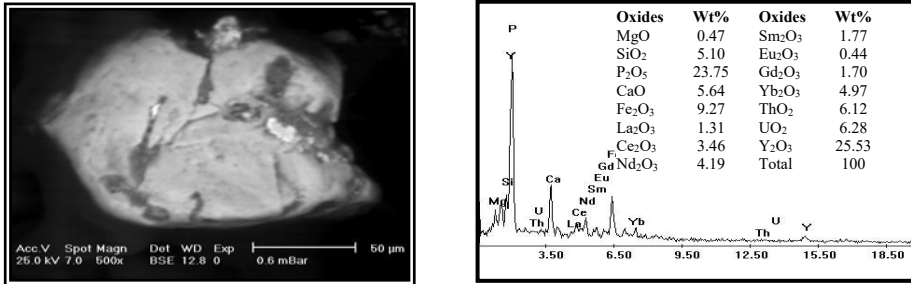
Fig. (29): BSE image and EDX of xenotime separated from beach sands of Ras Baghdady area, Red Sea coast, Egypt.

4.4- Apatite: Ca4[(Ca,F,Cl,OH])(PO4)3

Apatite exists as a minor constituent. Apatite is recorded as colorless to pale yellow, transparent, rounded pitted grains and occurs in oval and tabular shapes, with vitreous to resinous luster. The picked apatite mineral grains are confirmed by XRD patterns to be mainly fluorapatite $Ca_4(Ca,F)(PO_4)_3$ mineral similar to the rounded colorless zircon grains under binocular microscope (Fig. 30).

Fig. (30): Photomicrograph, BSE image and EDX of apatite separated from beach sands of Ras Baghdady area, Red Sea coast, Egypt.

4.5- Corundum: Al2O3

Corundum is recorded as a trace amount among the economic mineral assemblage in the studied beach sands of Ras Baghdady area. Corundum grains occur in rounded edges barrel-shaped habit. The fracture of the mineral is conchoidal or uneven. The mineral possesses a vitreous to adamantine luster. Its color varies from grey to various shades of blue or purple tints (Fig. 31).
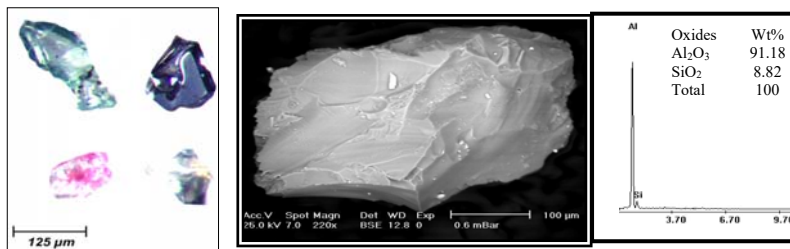

Fig. (31): Photomicrograph, BSE image and EDX of corundum separated from beach sands of Ras Baghdady area, Red Sea coast, Egypt.

Computation of the economic heavy minerals contents:

The weight percent of each mineral in every sub-fraction (Q) is calculated using the equation of Strakhov *et al.* (1957):

$$Q = \frac{\rho nd.100}{P(\sum nd)}$$

Where (ρ) is the weight of the magnetic subfraction, (P) is the weight of the total heavy fraction (table, 1), (n) is the number of grains and (d) is the specific gravity. The determined specific gravity values for the different minerals given by Hammoud (1973) were used. The volume of the beach sands of Ras Baghdady area is calculated in m^3 as multiplying area by depth. The studied area is measured using VistaMetrix® program version 1.35.0. This software runs as a transparent window using a Google Earth image. As the measured area is 5.52 km^2 and the depth of sampling is 2 m in average, the present estimation shows that, the studied beach sand of Ras Baghdady area contain 1104 × 10^4 m^3 of raw sands. The calculated apparent density varies from (1.25 – 1.71) g/cm^3 with an average of (1.5) g/cm^3 of the studied beach sand. The average bulk density of investigated sands is multiplied by the volume of the studied prospect to get the raw sands tonnage content. The investigated beach sands of Ras Baghdady area are about 16560 × 103 tons of bulk raw sands. The average content of the compromise size (0.125 - 0.063 mm) is about 11.33 wt.%. Therefore, the bulk raw sands comprise 1875.81× 103 tons of very fine sands. The average content of the total heavy minerals in this size fraction is 3.24 wt.%, so, the total heavy minerals is about 536.32×10^3 tons. The total economic minerals (T.E.M) content is about 45.29×10^3 tons. Besides, the gangue minerals are about 491.01×10^3 tons with content of about 2.92 wt.%. Gangue minerals comprise 479.52×10^3 tons of green silicate minerals and 11.5×10^3 of other minerals. Tonnage contents of individual economic minerals are shown in table (3). Meanwhile, the weight of each economic heavy mineral in gram (Table. 4) in the studied size fraction (0.125–0.063mm) of each sample is determined by multiplying its relative frequency (wt. %) by its total heavy minerals contents.

Table (3): Tonnage of economic minerals of the size grade (0.125-0.063 mm) in the studied beach sands of Ras Baghdady area.

Minerals	T.E.M*	Ilmenite	Magnetite	Garnet	Goethite	Zircon	Rutile	Sphene	Leucoxene	Green silicates	Others
Wt %	8.44	4.38	1.25	0.95	0.96	0.40	0.23	0.28	0.002	9.41	2.14
×10^3 tons	45.29	23.49	6.71	5.07	5.14	2.17	1.22	1.49	0.01	479.52	11.5

Distribution Analysis Of The Economic Heavy Minerals:

Concentration of heavy minerals by current waves was suggested to be controlled by topography of the beach. Wherein the topographic gradient affects the rate of erosion and reworking of sediments. Besides, the degree of hydraulic sorting of heavy minerals differs markedly between the upper and lower flow regimes. The total heavy minerals content tends to be more accumulated towards the southern limb of the studied area (Fig. 33). The northern portion of Ras Baghdady area lies nearby the

mouth of Wadi El Gemal at relatively high level. Meanwhile, the slope gradient decreases towards the southern portion (Fig. 32).

Lateral distribution of the economic heavy minerals:

Ilmenite represents the principal economic mineral (4.38 Wt.%) followed by amount of magnetite (1.25 wt.%) as economic minerals of the investigated beach placer deposits (Tables 3 & 4).

The calculated correlation coefficient values between the different heavy mineral contents across each individual profile reveals that both rutile and zircon have significant positive correlation with each other across the "A" (r = 0.91), "B" and "C" (r = 0.99) profiles. This is probably controlled by the hydraulic ratios and the shape-fractionation index (Fig. 34). Whereas, the degree of correlation between hydraulic ratios of rutile and zircon across the profile A is 0.92 and across B and C is 0.99.
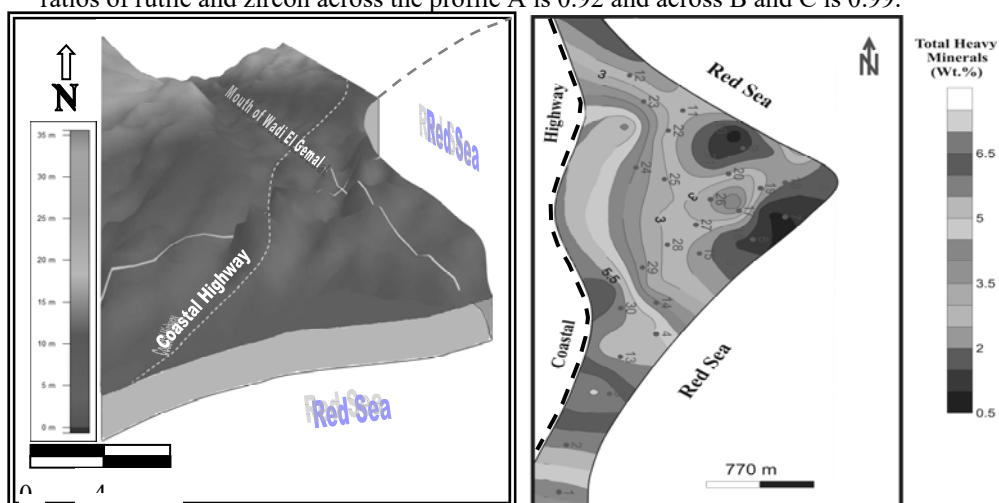

Fig. (32): Block diagram shows topography of Ras Baghdady area.

Fig. (33): Isoconcentration lines map shows distribution of total heavy minerals (THM) in Ras Baghdady area.

Despite both of rutile (0.23 wt. %) and zircon (0.4 wt . %) show relatively low abundant content, they depict a significant positive correlations with ilmenite, the highest recorded mineral within the studied samples across the profiles "A" (where; r = 0.63 and 0.83 respectively) and "C" (where; r = 0.81 and 0.82 respectively). These indicators suggest that ilmenite, rutile and zircon representing the major mineral association of the total economic mineral assemblage. This can be explained by their resistant character to chemical weathering.

Besides, across the profile B; each of ilmenite, rutile and zircon exhibit confident and significant correlation with goethite (r = 0.65, 0.69 and 0.70 respectively). Meanwhile, both rutile and zircon shows strong correlation with garnet (r = 0.71 and 0.72 respectively) and very strong correlation with sphene (r = 0.95 and 0.94 respectively). Moreover, garnet shows very strong correlation with goethite (r = 0.83). These strong to very strong correlation degrees assign to that, the overall economic heavy minerals concentrations chiefly controlled by their hydraulic ratio values.

Whereas concentrations of the economic heavy minerals are strongly correlated with their hydraulic ratio values, so the samples with larger hydraulic ratio values for each economic mineral indicate areas where the mineral was relatively more available for deposition and accumulations.

Therefore, the constructed maps of isoconcentration lines show that contents of ilmenite, rutile, zircon and sphene increase toward the southern part of the study area. Meanwhile, the northern part has relatively lower contents of these minerals. Uniformity of their distribution patterns reflects the strong to very strong correlation between their contents and their hydraulic factor values (Fig. 35).

Moreover, high contents of magnetite is recorded toward the extreme northern and southern parts of the triangular apex of the studied area, while the extensive central part is dominated by low contents. Moreover, goethite shows erratic to gradational distribution manner across the study area. Meanwhile garnet exhibits irregular distribution indicated by its low contents throughout the whole area with abrupt rising at its extreme southern part (Fig. 36).

Table (4): Contents of heavy minerals in grams within the grain size interval 0.063–0.125 mm.

Minerals S. No	Ilm.	Mag.	Gar.	Goet.	Zr.	Rut.	Sph.	G. S.
1	0.479	0.106	0.061	0.051	0.027	0.011	0.005	2.872
2	0.583	0.151	0.625	0.079	0.038	0.012	0.026	3.813
3	0.399	0.189	0.032	0.079	0.019	0.014	0.029	6.229
4	0.716	0.124	0.079	0.064	0.096	0.031	0.018	3.867
5	0.036	0.005	0.022	0.023	0.004	0.003	0.010	1.472
6	0.091	0.002	0.015	0.002	0.007	0.002	0.000	0.863
7	0.076	0.002	0.033	0.017	0.014	0.009	0.014	1.675
8	0.039	0.037	0.003	0.011	0.001	0.002	0.003	1.401
9	0.071	0.053	0.008	0.040	0.004	0.005	0.010	4.018
10	0.078	0.037	0.011	0.026	0.004	0.007	0.009	3.513
11	0.061	0.139	0.006	0.016	0.005	0.004	0.004	2.538
12	0.029	0.023	0.002	0.007	0.002	0.001	0.001	1.099
13	0.123	0.085	0.041	0.074	0.090	0.052	0.077	4.522
14	0.137	0.051	0.007	0.030	0.007	0.006	0.011	2.853
15	0.126	0.013	0.016	0.050	0.020	0.012	0.009	2.562
16	0.224	0.008	0.034	0.057	0.005	0.004	0.012	4.124
17	0.057	0.010	0.006	0.021	0.002	0.003	0.008	2.952
18	0.073	0.005	0.008	0.035	0.001	0.002	0.009	3.799
19	0.024	0.022	0.003	0.011	0.001	0.000	0.000	1.826
20	0.019	0.002	0.001	0.006	0.001	0.000	0.000	0.651
21	0.059	0.010	0.003	0.021	0.002	0.001	0.005	2.289
22	0.058	0.054	0.004	0.018	0.005	0.004	0.007	1.850
23	0.029	0.024	0.000	0.012	0.001	0.001	0.003	1.441
24	0.105	0.014	0.000	0.056	0.004	0.005	0.013	5.219
25	0.040	0.002	0.000	0.049	0.001	0.002	0.003	2.854
26	0.018	0.005	0.000	0.013	0.002	0.001	0.002	1.474
27	0.041	0.029	0.019	0.021	0.005	0.001	0.000	2.794
28	0.220	0.014	0.048	0.026	0.007	0.005	0.003	2.492
29	0.341	0.028	0.016	0.027	0.051	0.033	0.005	3.076
30	0.534	0.089	0.077	0.047	0.045	0.026	0.012	5.319
Min.	0.018	0.002	0.000	0.002	0.001	0.0001	0.0001	0.651
Max.	0.716	0.189	0.625	0.079	0.096	0.052	0.077	6.229
Average	0.163	0.044	0.039	0.033	0.016	0.009	0.010	2.849
S.D.	0.191	0.051	0.113	0.022	0.025	0.012	0.014	1.390

Ilm. = Ilmenite; Mag. = Magnetite; Zr. = Zircon; Rut. = Rutile; Gar. = Garnet; Goet. = Goethite;
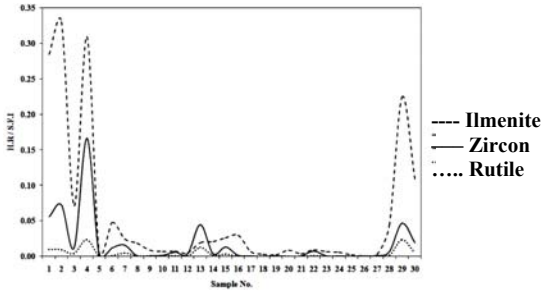G.S. = Green silicate minerals.

Fig.(34):Diagram shows the strong relationship between hydraulic factors of ilmenite, zircon and rutile in the size interval (0.125–0.063mm) of the studied samples. (H.R. = Hydraulic ratio; S.F.I. = Shape-fractionation index).
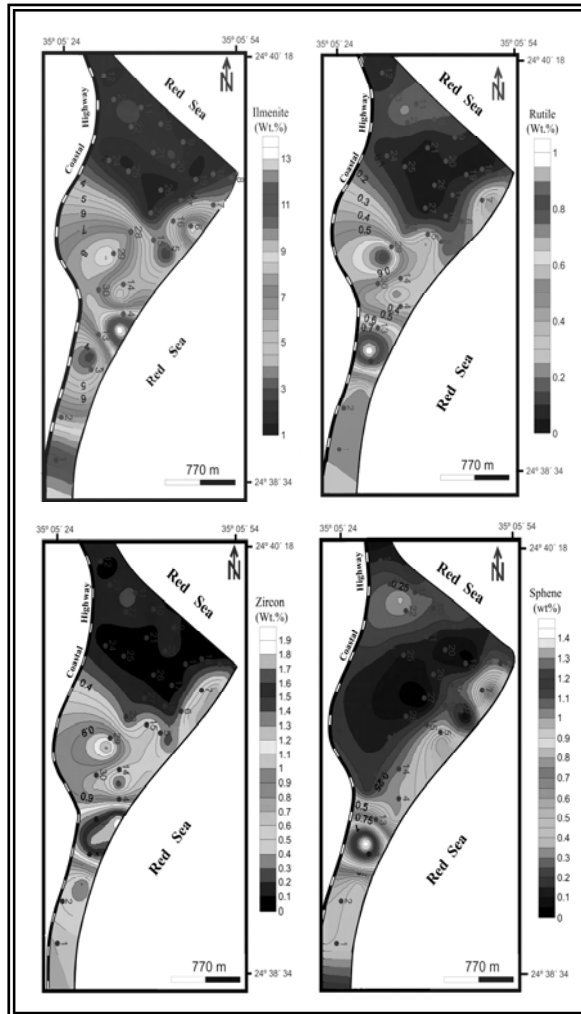

Fig.(35): Isoconcentration line maps show distribution of ilmenite, rutile, zircon and sphene in Ras Baghdady area. (N.B. The light colors point to the highest content.)
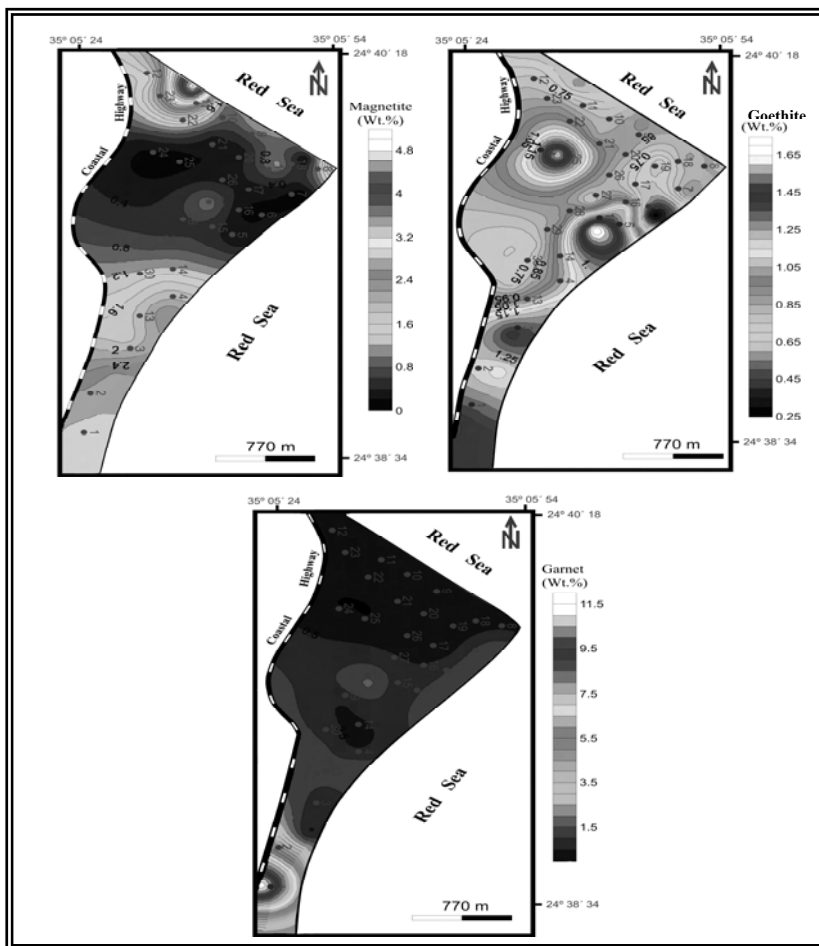
Fig.(36): Isoconcentration line maps show distribution of magnetite, goethite and garnet in Ras Baghdady area. (N.B. The light colors point to the highest content.)

Conclusion

1. The recorded heavy minerals; 90 % of green silicates and 10 % of heavy minerals; ilmenite, magnetite, garnet, goethite, zircon, rutile, sphene and other 2 % combined mineral traces from Ras Baghdady very fine sand size (0.125 - 0.063 mm). The total recorded heavy minerals ranges from 0.69 to 7.12 wt. % with 3.24 wt. % in average. The opaque minerals include ilmenite, magnetite and goethite forming about 71 % of the total detected heavy minerals. The non-opaque heavy minerals orthosilicates; garnet, zircon, sphene and translucent rutile form about 29 % of the total heavy minerals. Radioactive elements and rare metals bearing minerals monazite, xenotime, uranothorite, apatite, cassiterite and corundum are

also recorded. The gangue minerals include green and colored silicate minerals.

2. Most of the studied heavy mineral grains are angular to sub-angular and homogenous in composition with a few variations due to short distance transportation and low energy deposition as depicted from the magnetically separated ilmenite grade III. Both of magnetically separated ilmenite grades I and II grains suffered from hematization depicting varicolored stains pointing to ilmenite-hematite ex-solution of solid solution phase (i.e. hematite lamellae in ilmenite host grain). The magnetite suffered from martitization, hematization and maghamitization to reflect exsolved titaniferous alterations. Further, zircon concentrates are either colored or colorless grains in which fluorapatite and hematite are recorded.

3. The relative abundances and lateral distributions of the economic heavy minerals assemblage in the studied area are mainly controlled by hydraulic effects and beach topography whereas the heavy minerals tend to be more accumulated towards the lower altitudes southern limb of Ras Baghdady raised beach far from Wadi El Gemal mouth. In this respect, significant correlation between ilmenite, rutile and zircon are obviously recorded.

4. The estimated reserve of the economic heavy minerals can be summed up as follow; Ilmenite 23490 tons, Magnetite 6710 tons, Garnet 5070 tons, Goethite 5140 tons, Zircon 2170 tons, Rutile 1220 tons, Sphene 1490 tons and Leucoxene 10 tons.

5. In addition to first recorded ruby and saphire, the rare metal and radioactive elements bearing minerals such as monazite in which rare earth elements reach 61.2 %, ~ 6.70 % Th, and ~ 5.4 % U as well as high content of Nd (17. 3%) and Sm (4.37%) are also recorded. Furthermore, the picked uranothorite grains show high content of Th (40.12 %), U (11.77 %), and Y (11.9 %) while xenotime contains high content of Y_2O_3 (25.53 %), Yb_2O_3 (4.97 %), Nd_2O_3 (4.19 %) and Ce_2O_3 (3.46 %) as well.

6. The recorded aluminum gem related minerals coulel be. ruby and saphire in the studied heavy fractions of the beach black sand point to probable presence of other valuable minerals (e.g.) in the upstream rocks. Thus, bed rock and stream sediments survey of the highly metamorphosed rock units located in the upstream area is recommended.

7. The recorded uranothorite, xenotime and monazite in these heavies point to probable presence of radioactive mineralization in upstream granitic rocks . Thus, the bed rock survey of the granitic and pegmatitic rocks located in the upstream area is also recommended.

References

1. ABU HALAWA A., MASOUD M., SHAHIN H., and EMBABY A., (2010): Economic and radioactive heavy minerals of El Hebal sand dunes, Southern Eastern desert, Egypt: Geologic Survey of Egypt.

2. ABU HALAWA, A., (2005): Evaluation and mineral processing of some economic minerals in El Burullus Baltim sand dunes, Nile Delta, Egypt. Ph.D. Thesis, Fac. Sci., Mansoura Univ., Egypt, 205 pp.

3. ASSAF, H. S., IBRAHIM M. E., ZALATA A. A., METWALLY A. A. and SALEH G. M. (2000): Polyphase folding in Nugrus – Sikeit area South Eastern Desert, Egypt. Earth Sci., V. 12, p. 1-16.

4. CARVER, R. E. (1971): Procedures in sedimentary petrology. Handbook, New York, Wiley, 653 P.

5. DABBOUR G. A.; MORSY M. A. and EL HADRY A. F. (1999) Occurrence of black sand with potential nuclear elements along the southern part of the Egyptian Red Sea Coast. 1st Semin. Nucl. Raw Materials and others Tech. Cairo. (abstract).

6. DILL, H. G. (1998): A review of heavy minerals in clastic sediments from the alluvial fan through the near shore. Earth science review (1998). el Sevier Science B. V.

7. EL AFANDY A. H.; ABU HALAWA A. and KANDIL M. K. (2011): Heavy mineral potentiality of beach placer deposits of south Ras Banas, Red Sea coast, Egypt: Sedimentology of Egypt, vol., 19. .

8. EL HADARY A. F. (2008): Sedimentological and mineralogical signature of Wadi El Gemal beach sediments, South Eastern desert, Egypt: Scientific J. of Fac. Sc. Menufiya Univ., Egypt.

9. EL KAMMAR A. M.; ARAFA I. H. and EL SHELTAMI O. R. (2007): Mineral composition and environmental geochemistry of the beach sediments along the eastern side of the Gulf of Suez, Egypt. Journal of African Earth Sciences Volume 49, Issue 3, October 2007, Pages 103-114.

10. EL SHAZLY, E. M. and HASSAN, M. A. (1972): Geology and radioactive mineralization at Wadi Sikait - Wadi El Gemal area, Eastern Desert, Egypt. J. Geol., 16 (2), 201-234.

11. HAMMOUD, N. M. (1966): Concentration of monazite from Egyptian black sands employing industrial techniques, M.Sc. Thesis, Fac. Sci. Cairo Univ. 201P.

12. HAMMOUD, N. M. (1973): Physical and chemical properties of some Egyptian beach economic minerals in relation to Thesis concentration problems. Ph. D. thesis, Fac. Sci. Cairo Univ. 302 P.

13. HASSAAN, M. M. (2011): Some metallic mineral deposits of the Nubian shield in Egypt. Handbook, 1st edition, Germany.

14. HUGO, V. E., and D. H. CORNELL. (1991): Altered ilmenites in Holocene dunes from Zululand, South Africa. Petrographic evidence for multistage alteration. S. Afr. J. Geol. 94(5/6): 365-378.

15. HUTTON, C. O. (1950): Studies of heavy detrital minerals. Bull. Geol. Soc. Amer. 61, 635 – 710.

16. IBRAHIM, T. M.; ABU HALAWA, A.; ALI, K. G. and GAAFAR, I. M. (2009): Occurrence of black sand deposits on the Red Sea coastal plain of Wadi Diit, South Eastern Desert, Egypt: A preliminary study. Sed. Egypt, Vol. 17, p.107 – 116.

17. KHALID, F. M. (2005): Geologic evaluation of some rare metal resources in Nugrus – Sikait area, Eastern Desert, Egypt. Ph.D. Thesis, El Azhar Univ. Egypt, 187 P.

18. KITAISKY, Y. D. (1963): Prospecting for minerals. Mir publishers, Moscow (1963).

19. MILNER, H. B. (1962): Sedimentary Petrology. George Allen & Unwin Ltd, London volume I, p. 112.

20. MUCKE A. and RAPHAEL A. (2005): Redox and nonredox reactions of magnetite and hematite in rocks. Chemie der Erde - Geochemistry. Volume 65, Issue 3, 20 July 2005, Pages 271–278

21. RAMADAN, T. M. and HODA M. O. (1999): Use of ERS-2 SAR and Landsat TM Images for geological mapping and mineral exploration of Sol Hamid area, South Eastern Desert, Egypt.

22. SALEH, G. M. (1997): The potentiality of uranium occurrences in Wadi Nugrus area, South Eastern Desert, Egypt. Ph.D. Thesis, Mansoura univ. Egypt, 171p.

23. STRAKHOV, N. M., BUSHINSKII, G. I. and PUSTOVALOV, L. V. (1957): Metody izocheniya ocadochnykh porod, tom I (Methods of studying sedimentary rocks, vol. I) Moskva, Gosgeoitekhiz dat, 611 pp.

24. SURESH BABU D. S., THOMAS K. A., MOHAN DAS P. N., and DAMODARAN A. D. (1994): alteration of ilmenite in the M a n a v a l a k u r i c h i deposit, Indi. Clays and clay minerals, vol. 42, no. 5, 567-571, 1994 .

25. YOUSRIA, M. S. and EL GOHARY, A. M. (2005): Mineralogical composition of the coastal sediments between Hurghada and El Qusier, Red Sea Coast. Sed. Egypt, Vol. 13, p.115 – 132.

26. WONG, F. L., (2001): Heavy minerals from Palos Verdes margin, Sothern california: data and factor analysis, open file report 1-153, 2001. US geological Survey. Internet zone.